Effect of Tensile Stress on Self-Magnetic Leakage Field in Carbon Steel Pipe Material

Nur Akmal Hakim Jasni[1,*], Mohamed Azlan Suhot[1], Mohd Hisham Abu Bakar[2], Aishah Mastura Supian[2]

1   Razak Faculty of Technology and Informatics, University Teknologi Malaysia, Jalan Sultan Yahya Petra, 54100, Kuala Lumpur, Malaysia
2   Engineering Department, Group Technical Solutions, Project Delivery & Technology Division, PETRONAS, Malaysia

ARTICLE INFO

ABSTRACT

Metal magnetic memory (MMM) technique is a promising non-destructive technology for determining the state of material deformation and structural defect in carbon steel pipe by measuring the self-magnetic leakage field (SMLF). The relationship between SMLF and stress concentration of cracked specimens has been extensively researched, but little is known about corrosion defects in carbon steel pipes, such as circular holes. A static tensile test and MMM measurement were performed on the ASTM A106 Gr. B steel to investigate its applicability in predicting material deformation state and structural defect. The tensile load makes the distribution of self-magnetic leakage field, SMLF intensities in the elastic stage regular. In the defect zone of defective specimens, a peak-trough in the SMLF intensity in the tangential component, Hp(x), and a peak in the normal component, Hp(y), were observed. As yield approached, the SMLF intensities remained unchanged. During plastic deformation, dislocation slip and dislocation interaction rarely change the SMLF intensities and its gradient. The SMLF intensities and its gradient rise as the tensile load approach its ultimate strength. The distribution of SMLF intensities show a peak feature in the Hp(x), and a peak-trough in the Hp(y) as the specimen fractures. Variations in the magnetic and stress fields of carbon steel pipe are caused by structural defect. As a result, the SMLF intensity varies. The method described in this study can be applied to MMM technique to detect material deformation states and defect formation in ASTM A106 Gr. B steel at low cost and with minimal equipment.

1. Introduction

Carbon steel pipeline is an important infrastructure used worldwide to transport crude oil or natural gas over long distances to meet the increasing demands of energy. It has been showed that the carbon steel pipeline is an effective and safe vehicle for the oil and gas transportation [1-3]. The integrity of these carbon steel pipelines is of importance due to the explosive characteristic of gas and oil [4]. Corrosion is one of many common factors that could threaten the integrity of carbon steel

---

pipelines, resulting in a significant stress concentration [5]. Several indirect physical methods, including ultrasonic testing, permeation testing, and eddy current testing, are only sensitive to structural defects in ferromagnetic components and not to stress concentration or early damage [6].

The Metal Magnetic Memory (MMM) test method, first introduced by Dubov in 1994, is a new, robust, and rapidly expanding non-destructive testing (NDT) technique. Metal magnetic memory (MMM) approaches have demonstrated to be successful in assessing stress concentration and defects in ferromagnetic materials as a unique magnetic testing method [7-9]. The failure condition of a structure can be assessed by detecting metal magnetic signal on the failure area and stress concentration zone [10, 11]. Due to its low cost and ease of implementation, this strategy has received considerable attention in engineering [12].

Many researchers contributed to the establishment of the correlation of self-magnetic leakage field, SMLF responses with ferromagnetic material deformation states in experimental fields. According to previous research, the SMLF intensities of ferromagnetic materials are random in the absence of stress [13], but they change to linear pattern as the stress increases in elastic state [14-16]. The SMLF intensities vary on a small scale once the applied stress reaches the yield point and plastic deformation state [17, 18]. A sharp change of $H_p(y)$ signal from negative to positive values and a zero-crossing point at the fracture location [12-19]. The findings of previous research have focused on the influence of material deformation states on SMLF intensities in the normal component, as compared to both the normal and tangential components.

Bao *et al.,* [18] stated that the characteristics of the abnormal distribution of SMLF intensities of 30CrNiMo8 steel can be used to find the exact location and shape of a defect. Xu *et al.,* [20], who investigated the response of SMLF intensities on a cracked Q345 steel specimen subjected to tensile load, the authors found that the peak and peak trough appears in the tangential and normal components, respectively. Liu *et al.,* [21] were among a few researchers who investigated the SMLF responses on pipeline material of API 5L X80 with a crack when subjected to internal pressure. According to the authors, the SMLF intensities of API 5L X80 steel in the stress concentration at the defective location is reasonably larger than the no-stress concentration area. While many researchers have studied the relationship between SMLF and stress concentration of cracked specimen, research into carbon steel pipe with corrosion defect such as circular hole is still limited.

For these interests, the work presented here focuses on the effect of deformation states on SMLF intensities in non-defective and defective ASTM A106 Gr. B steel specimen with crack and circular hole. The variations of SMLF intensities in normal and tangential component and its gradient throughout the entire tensile process for non-defective and defective specimens were presented and analyzed. The relationship between the SMLF measured by MMM technique and material deformation states and structural defect in ASTM A106 Gr. B steel will be important in analyzing the integrity of carbon steel pipes at a low cost and with minimal equipment.

2. Methodology
2.1 Specimen

The experiment in this study used ASTM A106 Gr. B steel, which is widely used as pipeline material. Table 1 and 2 indicate its chemical composition and mechanical properties, respectively. The specimens were cut from a pipe and machined into a dog-bone shape as illustrated in Figure 1. There are two types of specimens: non-defective and defective with circular hole in the middle. All specimens were demagnetized using a VERTEX VDM-8 demagnetizer model to randomize the initial magnetic state.
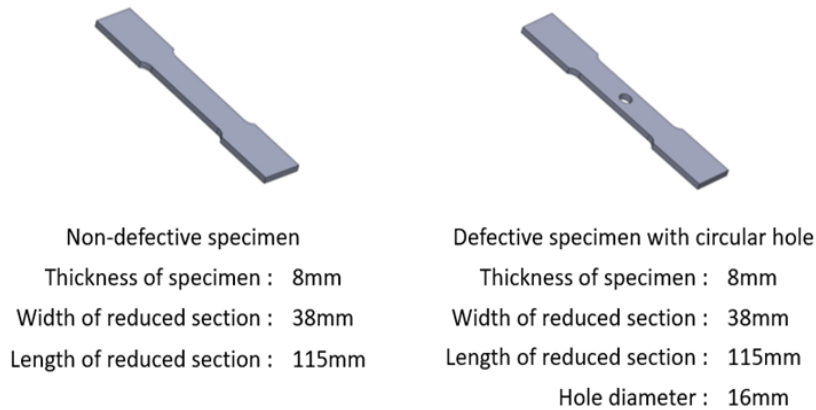
Table 1
Chemical composition of ASTM A106 Grade B steel (weight %) [22]

C	Mn	P	S	Si	Cr	Fe	Cu	Mo	Ni	V
0.3	0.29	0.04	0.04	0.1	0.4	97	0.4	0.15	0.4	0.08

Table 2
Mechanical properties of ASTM A106 Grade B steel

Yield strength (MPa)	Ultimate strength (MPa)
240	415

Non-defective specimen
Thickness of specimen : 8mm
Width of reduced section : 38mm
Length of reduced section : 115mm

Defective specimen with circular hole
Thickness of specimen : 8mm
Width of reduced section : 38mm
Length of reduced section : 115mm
Hole diameter : 16mm

Fig. 1. Non-defective and defective tensile specimen dimensions

2.2 Experimental Procedure

The specimen was placed vertically between the grips as shown in Figure 2, and the static tensile test was carried out at room temperature on a ZwickRoell Z400E Standard Universal Testing Machine with a maximum static load of 400kN. The specimen was first loaded at a tensile rate of 0.2mm/min to a preset value and held for a period of time throughout the tensile testing. The $H_p(x)$ and $H_p(y)$ were then measured immediately along the 100mm scanning line with a 1mm scanning interval using a TSC-7M-16 type magnetometer developed by Energodiagnostika Co. Ltd. The gradient of SMLF intensities in tangential and normal component, $dH_p(x)/dX$ and $dH_p(y)/dX$ will be calculated accordingly. The specimen was then loaded to a higher predetermined value and the process continued until it fractured. The specimens went through the entire failure process, including elastic deformation, plastic deformation and fracture as shown in Figure 3.
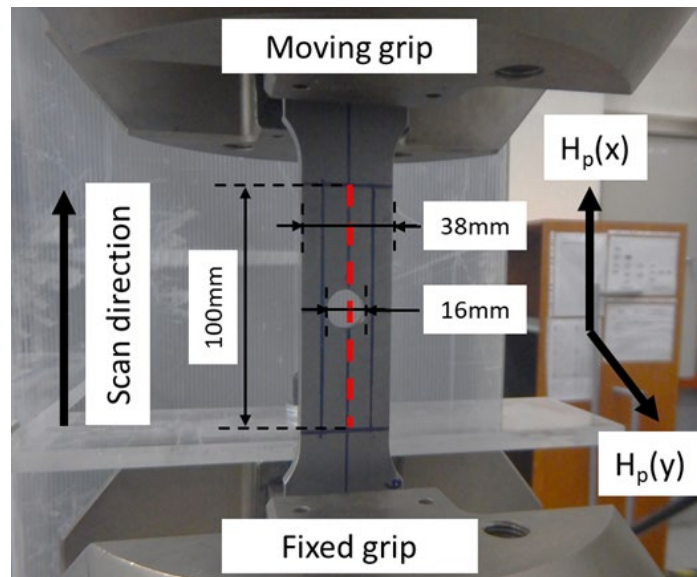
**Fig. 2.** Experimental set-up for static tensile test with MMM measurement
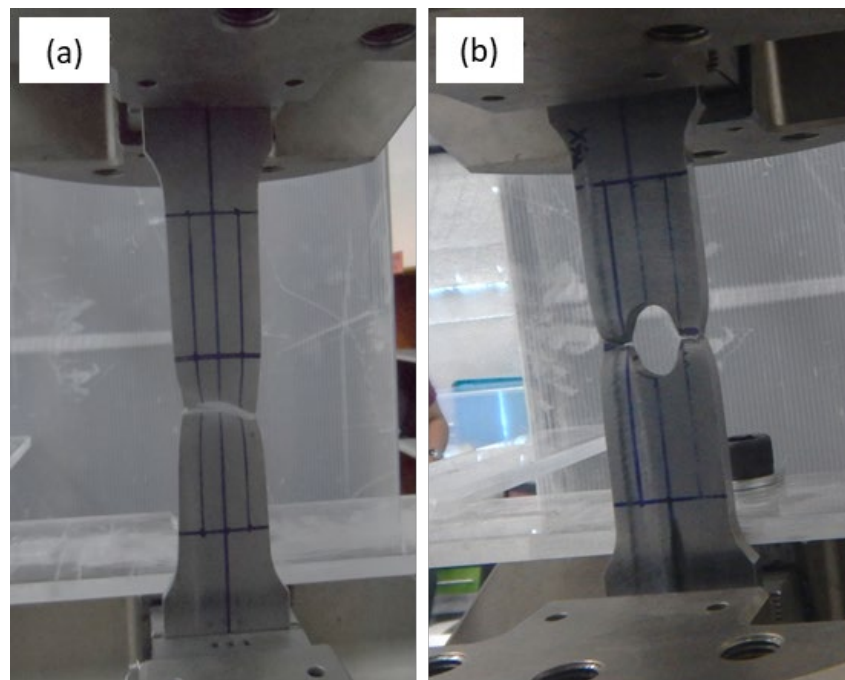
Fig. 3. Fractured photo of (a) non-defective and (b) defective specimen

## 3. Results and Discussion

3.1 Elastic State

$H_p(x)$ distribution has a negative slope before applying tensile loading corresponding to 0kN as depicted in Figure 4(a), whereas $H_p(y)$ has a parabola trend with the minimum value in the centre as shown in Figure 4(b) for all specimens, which is similar to the previous work's findings [23]. The initial SMLF intensities could be linked to the history of specimen machining [13] and specimen micro-inhomogeneity [24, 25].
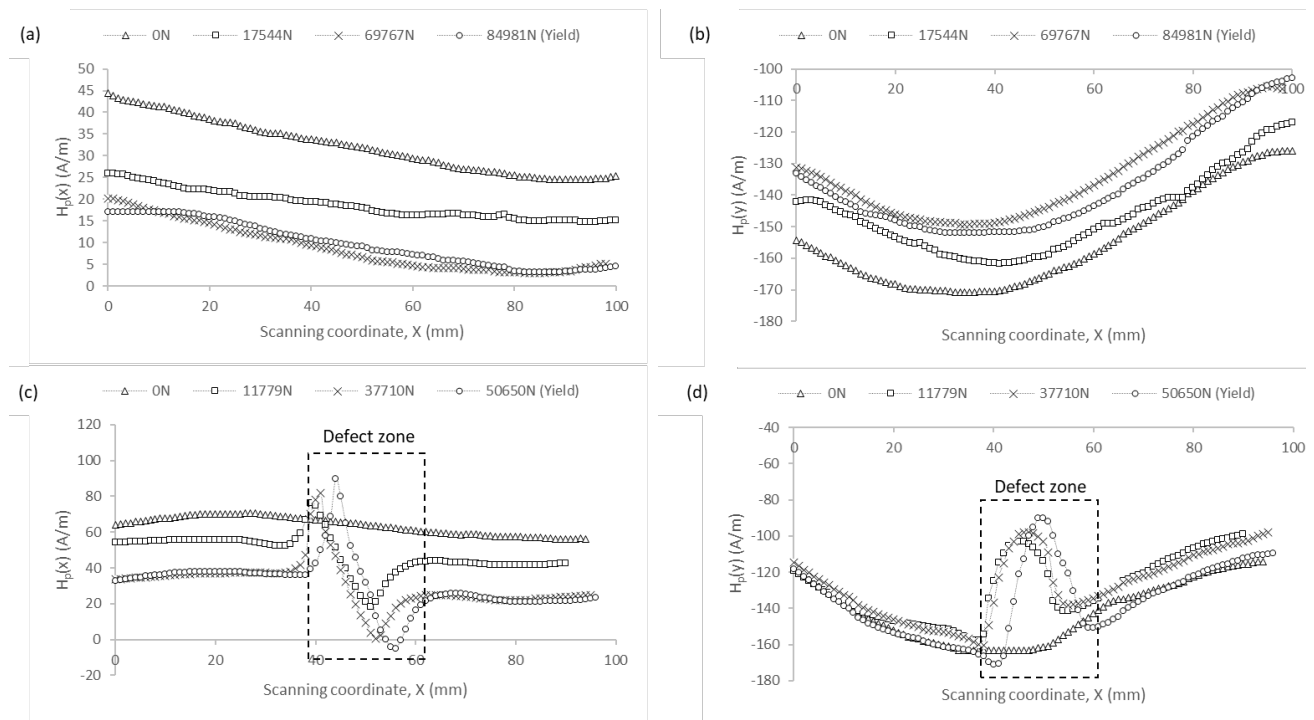
Fig. 4. SMLF intensity distributions at the elastic state of (a) $H_p(x)$ of non-defective specimen (b) $H_p(y)$ of non-defective specimen, (c) $H_p(x)$ of defective specimen and (d) $H_p(y)$ of defective specimen

The $H_p(x)$ and $H_p(y)$ of the defective specimen with a circular hole change to a peak-trough and peak feature as the tensile test progresses, as shown in Figure 4(c) and 4(d), respectively, which is similar to previous work [26]. Both $H_p(x)$ and $H_p(y)$ are sensitive to the abnormal magnetic changes caused by the local stress concentration in the defect area [27]. The self-magnetic leakage field in a specimen under tensile stress varies depending on whether it is non-defective or defective. As a result, the $H_p(x)$ and $H_p(y)$ are distinct [28]. According to Fu *et al.,* [27], the abnormal magnetic change in the defect zone can be explained by magnetic-charge theory. The defective specimens cause a significant change in magnetic behaviour due the magnetization effect of the applied load and the Earth's magnetic field.

The defect zone can also be correlated to the $dH_p(x)/dX$ and $dH_p(y)/dX$ distributions where it shows peak feature as depicted in Figure 5 due to the variation in the SMLF intensities. The length of the abnormal feature in $dH_p(x)/dX$ and $dH_p(y)/dX$ is comparable to the diameter of the circular hole. As the tensile load increases, the amplitude of $dH_p(x)/dX$ and $dH_p(y)/dX$ peaks also increases. The piezomagnetic effect causes the magnetic properties of the material to become stronger as the stress level rises [15, 29, 30], as the magnetic domain walls within the specimen are able to rotate freely and easily [17-19].
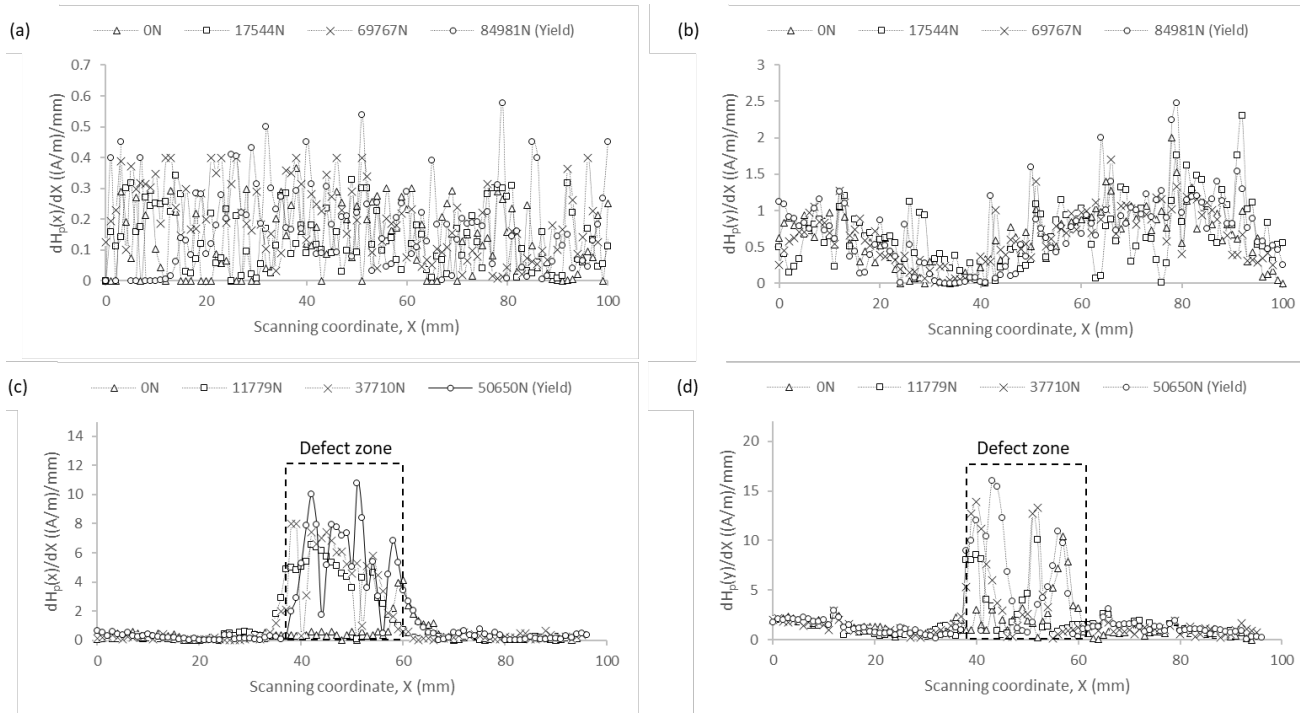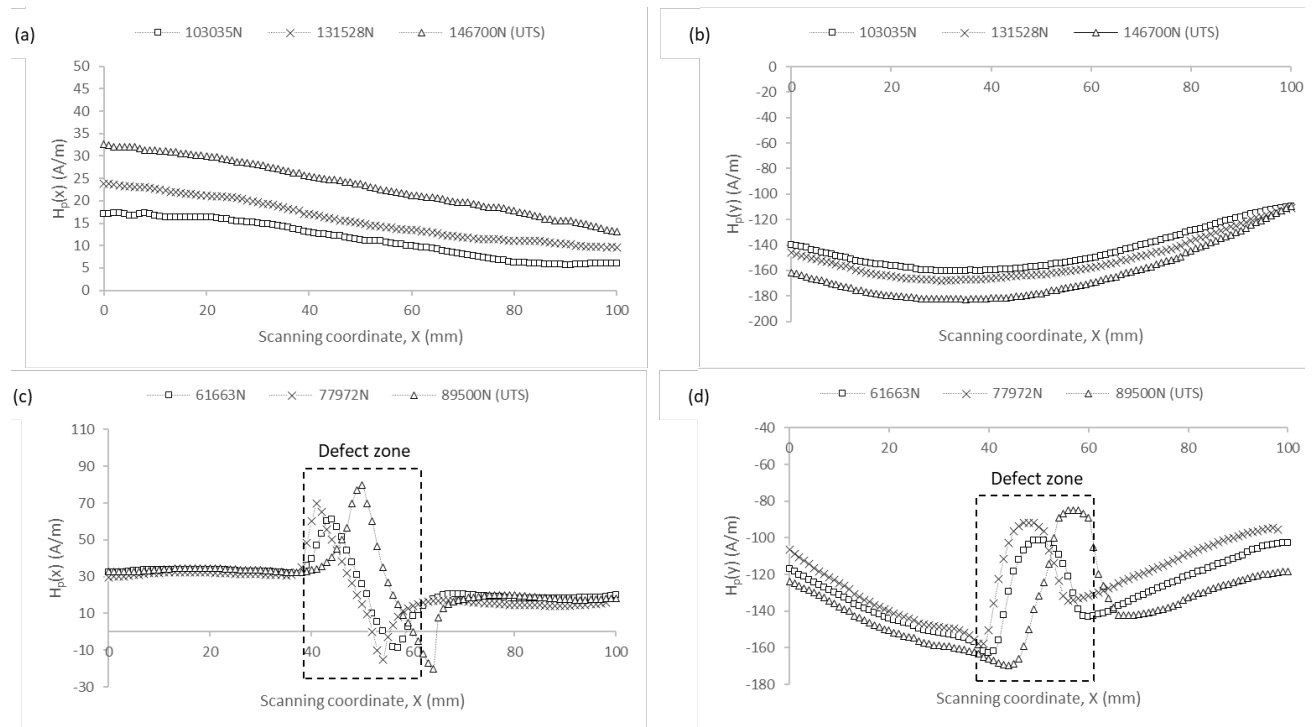
Fig. 5. Gradient of SMLF intensity distribution at the elastic state of (a) $dH_p(x)/dX$ of non-defective specimen (b) $dH_p(y)/dX$ of non-defective specimen (c) $dH_p(x)/dX$ of defective specimen and (d) $dH_p(y)/dX$ of defective specimen

As shown in Figure 4, there were no significant changes in $H_p(x)$ and $H_p(y)$ as the tensile stress reached the yield point. As the applied force approaches the yield point, the $H_p(x)$ and $H_p(y)$ features appear to reach their maximum value, and they rarely change as the applied load increases [14, 31, 32]. According to Liu *et al.,* [30], as stress exceeds yield strength, dislocation pinning occurs on the magnetic domain, constraining magnetic domain orientation change. Su *et al.,* [15] reached the conclusion that SMLF intensities can indicate whether a ferromagnetic material is yielding.
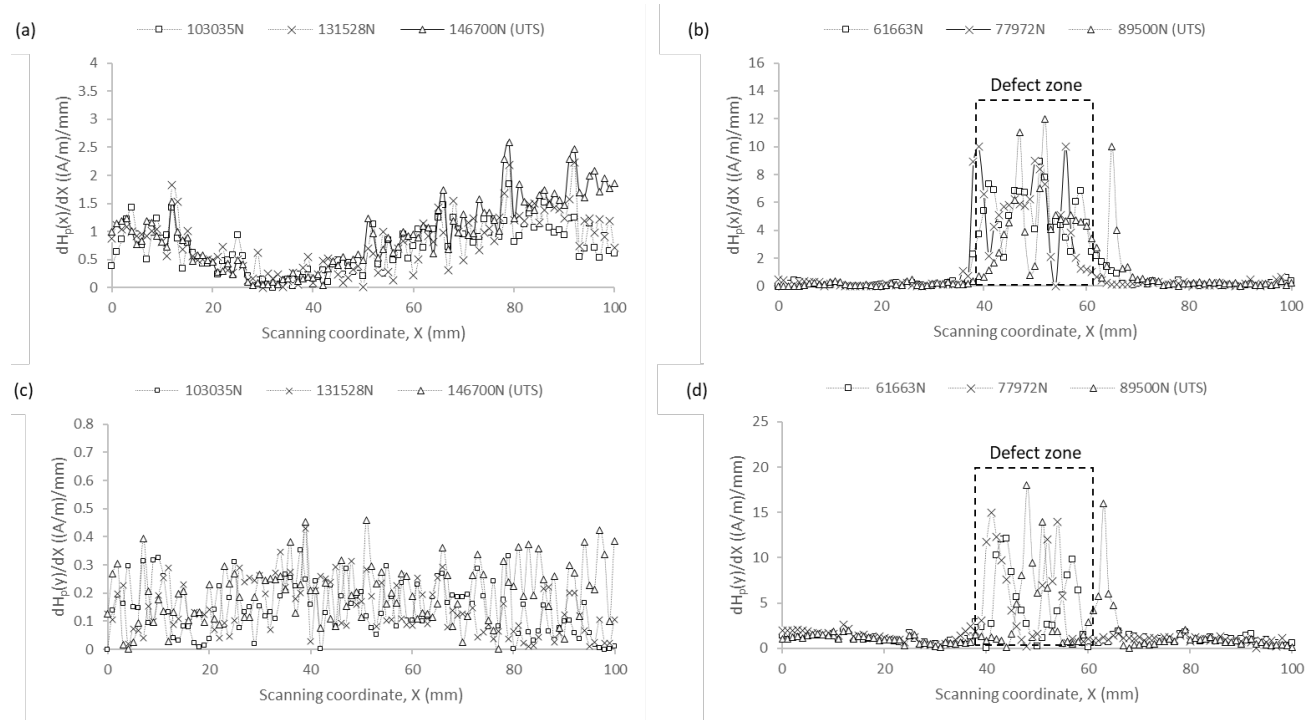
3.2 Plastic Deformation State

With increasing tensile stress during plastic deformation, the SMLF intensities and gradient fluctuations in $H_p(x)$ and $H_p(y)$ are barely changed especially between 103035N to 131528N for non-defective specimen and 61663N to 77972N for defective specimen as demonstrated in Figure 6. Ren and Ren [16] claimed if the maximum tensile stress exceeds the yield point, the magnetic induction intensity fluctuates relatively slightly. The metal crystal hardens due to dislocation slip and dislocation interactions. The dislocation's interaction reduces its range of motion and movement [19, 26].

The SMLF intensities in the tangential and normal components, as well as its gradients, increases as the tensile load approaches ultimate tensile strength (UTS) as depicted in Figure 6 and 7. Jian *et al.,* [33] and Kumar and Misra [34], who observed that raising the necking degree enhanced the gradient of SMLF intensities at the necking site, confirm this result. As the stress weakens the pinning impact of dislocation on the magnetic domain at the necking point, raising the stress concentration degree aided in increasing the gradient of SMLF intensities, indicating that the process of pinning the magnetic domain was not entirely stopped.
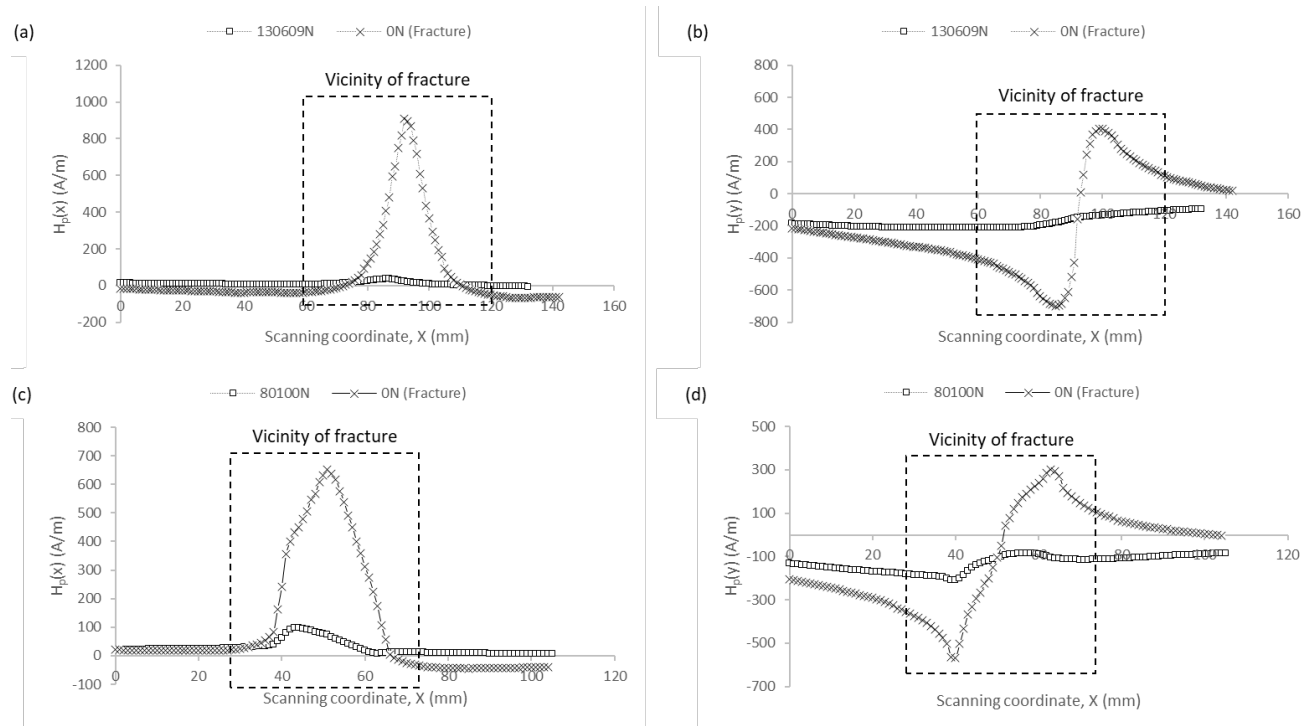
Fig. 6. SMLF intensity distributions at the plastic deformation state of (a) $H_p(x)$ of non-defective specimen (b) $H_p(y)$ of non-defective specimen (c) $H_p(x)$ of defective specimen and (d) $H_p(y)$ of defective specimen

Fig. 7. Gradient of SMLF intensity distribution at the plastic deformation state of (a) $dH_p(x)/dX$ of non-defective specimen (b) $dH_p(x)/dX$ of defective specimen (c) $dH_p(y)/dX$ of non-defective specimen and (d) $dH_p(y)/dX$ of defective specimen
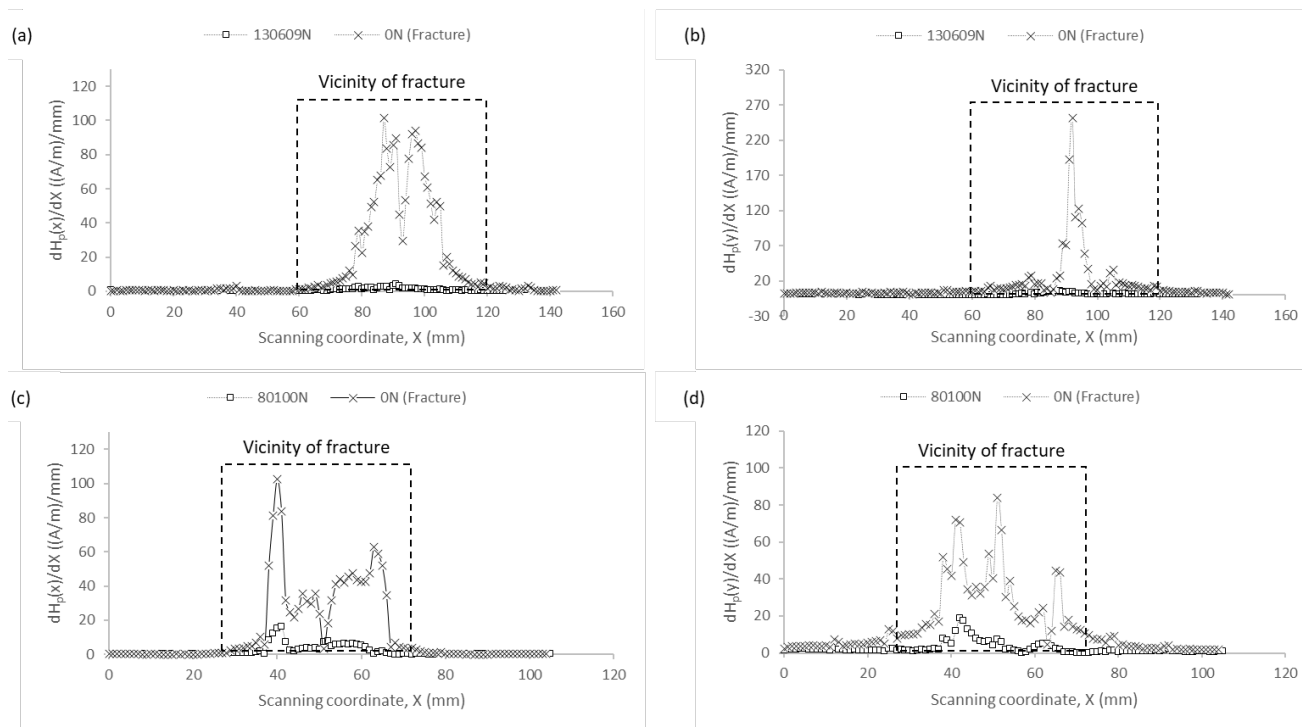
3.3 Fracture State

The $H_p(x)$ as the specimen fractures exhibits a peak, as shown in Figure 8(a) and 8(c), similar to the findings of Huang *et al.,* [35] and Hu *et al.,* [36]. Meanwhile, a peak-trough feature is seen in $H_p(y)$ as depicted Figure 8(b) and 8(d), which is comparable to the previous studies [26, 37] where the fractured ends had distinct and opposite poles (positive at the left fractured end and negative at the right fractured end).

Fig. 8. SMLF intensity distributions at the fracture state of (a) $H_p(x)$ of non-defective specimen, (b) $H_p(y)$ of non-defective specimen, (c) $H_p(x)$ of defective specimen and (d) $H_p(y)$ of defective specimen

Figure 9(a) and 9(c) demonstrates that the $dH_p(x)/dX$ has pronounced two peaks, while the $dH_p(y)/dX$ has a peak, as shown in Figure 9(b) and 9(d). After the fracture, the peak in $dH_p(x)/dX$ and $dH_p(y)/dX$ increased significantly, corresponding to the high variance in the SMLF intensities [12, 19, 26].

Fig. 9. Gradient of SMLF intensity distribution at the fracture state of (a) dH$_p$(x)/dX of non-defective specimen, (b) dH$_p$(y)/dX of non-defective specimen, (c) dH$_p$(x)/dX of defective specimen and (d) dH$_p$(y)/dX of defective specimen

4. Conclusions

Under different tensile loads, the variations of SMLF intensities and gradients on the surface of non-defective and defective ASTM A106 Gr. B specimens were studied. The following conclusions were derived from this study:

i. In the elastic stage, the distribution of SMLF intensity changes from random to regular pattern when subjected to a tensile load. The peak amplitude of gradient of SMLF intensity increases with tensile stress. This is due to the piezomagnetic effect, which strengthens the magnetic properties of a material when it is under stress. Tensile load reached yield strength with no noticeable changes in SMLF intensities because dislocation pinning restrains magnetic domain orientation shift.

ii. In the stage of plastic deformation, dislocation slip and dislocation interaction in the metal crystal affect the metal magnetic signals and its gradient. The interaction of the dislocation restricts its movement. As the tensile load approaches the ultimate tensile strength (UTS), raising the stress concentration reduced the pinning effect of dislocation on the magnetic domain, increasing the gradient of SMLF intensities. As the specimen fractures, the H$_p$(x) exhibits a peak feature, whereas the H$_p$(y) demonstrates a peak-trough. Due to the large variance in SMLF intensities, the peak amplitude of gradients increases.

iii. The stress distribution of non-defective and defective specimen with a circular hole are different under tensile loading. As a result, the SMLF intensities and its gradient are different. The abnormal features in the SMLF intensities and gradients indicate not only the location of the defect, but also the defect's length based on the length of the abnormal feature.

iv. The investigation of the SMLF responses to tensile stress in the ASTM A106 Gr. B steel has made a substantial contribution to the oil and gas industry, as the investigated material has been studied very little by other researchers despite its extensive use as pipe material in the pipeline systems. The findings of this study on material deformation can be utilized to determine material deformation states in carbon steel pipe, which is crucial for ensuring that pipeline systems are operated in an elastic state. Moreover, the abnormal feature in SMLF intensities and gradients of the circular hole can be used to detect the formation of corrosion defects on carbon steel pipe, such as pitting, pinholes, etc., which are commonly observed in pipeline systems.

Acknowledgement

References

[1] Gao, Jie, Pei Yang, Xin Li, Jing Zhou, and Jinkun Liu. "Analytical prediction of failure pressure for pipeline with long corrosion defect." *Ocean Engineering* 191 (2019): 106497. https://doi.org/10.1016/j.oceaneng.2019.106497

[2] Zhu, Xian-Kui. "A comparative study of burst failure models for assessing remaining strength of corroded pipelines." *Journal of Pipeline Science and Engineering* 1, no. 1 (2021): 36-50. https://doi.org/10.1016/j.jpse.2021.01.008

[3] Abyani, Mohsen, and Mohammad Reza Bahaari. "A new approach for finite element based reliability evaluation of offshore corroded pipelines." *International Journal of Pressure Vessels and Piping* 193 (2021): 104449. https://doi.org/10.1016/j.ijpvp.2021.104449

[4] Tee, Kong Fah, and Alvan H. Wordu. "Burst strength analysis of pressurized steel pipelines with corrosion and gouge defects." *Engineering Failure Analysis* 108 (2020): 104347. https://doi.org/10.1016/j.engfailanal.2019.104347

[5] Khan, Faisal, Rioshar Yarveisy, and Rouzbeh Abbassi. "Risk-based pipeline integrity management: A road map for the resilient pipelines." *Journal of Pipeline Science and Engineering* 1, no. 1 (2021): 74-87. https://doi.org/10.1016/j.jpse.2021.02.001

[6] Gao, W. X., Y. H. Hu, X. Y. Mu, and X. M. Wu. "Real-time detection and segmentation of submerged-arc welding defects in X-ray radiography images." *Chinese Journal of Scientific Instrument* 32, no. 6 (2011): 1215-1224. https://doi.org/10.1784/insi.2014.56.6.299

[7] Dubov, A. A. "Diagnostics of steam turbine disks using the metal magnetic memory method." *Thermal engineering* 57, no. 1 (2010): 16-21. https://doi.org/10.1134/S0040601510010039

[8] Dubov, A. A. "Development of a metal magnetic memory method." *Chemical and Petroleum Engineering* 47, no. 11-12 (2012): 837-839. https://doi.org/10.1007/s10556-012-9559-6

[9] Leng, Jiancheng, Yang Liu, Guoqiang Zhou, and Yatian Gao. "Metal magnetic memory signal response to plastic deformation of low carbon steel." *Ndt & E International* 55 (2013): 42-46. https://doi.org/10.1016/j.ndteint.2013.01.005

[10] Gao, Fumin, JianChun Fan, Laibin Zhang, Jiankang Jiang, and Shoujie He. "Magnetic crawler climbing detection robot basing on metal magnetic memory testing technology." *Robotics and Autonomous Systems* 125 (2020): 103439. https://doi.org/10.1016/j.robot.2020.103439

[11] Wang, Guoqing, Lijian Yang, Ping Yan, and Liwa Wei. "Test procedure for stress damage of ferromagnetic materials based on metal magnetic memory effects." *Materials Testing* 60, no. 3 (2018): 301-305. https://doi.org/10.3139/120.111151

[12] Ren, Shangkun, Xianzhi Ren, Zhenxia Duan, and Yuewen Fu. "Studies on influences of initial magnetization state on metal magnetic memory signal." *NDT & E International* 103 (2019): 77-83. https://doi.org/10.1016/j.ndteint.2019.02.002

[13] Dong, Li-hong, Bin-shi Xu, Shi-yun Dong, Qun-zhi Chen, Yu-ya Wang, Lei Zhang, Dan Wang, and Da-wei Yin. "Metal magnetic memory testing for early damage assessment in ferromagnetic materials." *Journal of Central South University of Technology* 12, no. 2 (2005): 102-106. https://doi.org/10.1007/s11771-005-0019-8

[14] Dong, Li-hong, Bin-shi Xu, Shi-yun Dong, Ming-hui Ye, Qun-zhi Chen, Dan Wang, and Da-wei Yin. "Metal magnetic memory signals from surface of low-carbon steel and low-carbon alloyed steel." *Journal of Central South University of Technology* 14, no. 1 (2007): 24-27. https://doi.org/10.1007/s11771-007-0005-4

[15] Su, Sanqing, Xuran Zhao, Wei Wang, and Xiaohui Zhang. "Metal magnetic memory inspection of Q345 steel specimens with butt weld in tensile and bending test." *Journal of Nondestructive Evaluation* 38, no. 3 (2019): 64. https://doi.org/10.1007/s10921-019-0603-8

[16] Ren, Shangkun, and Xianzhi Ren. "Studies on laws of stress-magnetization based on magnetic memory testing technique." *Journal of Magnetism and Magnetic Materials* 449 (2018): 165-171. https://doi.org/10.1016/j.jmmm.2017.09.050

[17] Pang, Caoyuan, Jianting Zhou, Ruiqiang Zhao, Hu Ma, and Yi Zhou. "Research on internal force detection method of steel bar in elastic and yielding stage based on metal magnetic memory." *Materials* 12, no. 7 (2019): 1167. https://doi.org/10.3390/ma12071167

[18] Bao, Sheng, Yibin Gu, Meili Fu, Da Zhang, and Shengnan Hu. "Effect of loading speed on the stress-induced magnetic behavior of ferromagnetic steel." *Journal of Magnetism and Magnetic Materials* 423 (2017): 191-196. https://doi.org/10.1016/j.jmmm.2016.09.092

[19] Huang, Haihong, Cheng Yang, Zhengchun Qian, Gang Han, and Zhifeng Liu. "Magnetic memory signals variation induced by applied magnetic field and static tensile stress in ferromagnetic steel." *Journal of Magnetism and Magnetic Materials* 416 (2016): 213-219. https://doi.org/10.1016/j.jmmm.2016.04.094

[20] Xu, Kunshan, Ke Yang, Jie Liu, and Yue Wang. "Study on metal magnetic memory signal of buried defect in fracture process." *Journal of Magnetism and Magnetic Materials* 498 (2020): 166139. https://doi.org/10.1016/j.jmmm.2019.166139

[21] Liu, Bin, Luyao He, Zeyu Ma, Hai Zhang, Stefano Sfarra, Henrique Fernandes, and Stefano Perilli. "Study on internal stress damage detection in long-distance oil and gas pipelines via weak magnetic method." *ISA transactions* 89 (2019): 272-280. https://doi.org/10.1016/j.isatra.2018.12.009

[22] Abdel-Karim, R., S. El-Raghy, M. Nabil, and Y. Reda. "Corrosion characteristics of ASTM A106 grade B carbon steel pipelines exposed to sodium sulfate solutions." (2018): 20180026. https://doi.org/10.1520/MPC20180026

[23] Sun, Le, Xin'en Liu, Dong Jia, and Hongpan Niu. "Three-dimensional stress-induced magnetic anisotropic constitutive model for ferromagnetic material in low intensity magnetic field." *Aip Advances* 6, no. 9 (2016). https://doi.org/10.1063/1.4964359

[24] Yao, K., B. Deng, and Z. D. Wang. "Numerical studies to signal characteristics with the metal magnetic memory-effect in plastically deformed samples." *Ndt & E International* 47 (2012): 7-17. https://doi.org/10.1016/j.ndteint.2011.12.004

[25] Leng, Jiancheng, Minqiang Xu, Guoqiang Zhou, and Zemin Wu. "Effect of initial remanent states on the variation of magnetic memory signals." *Ndt & E International* 52 (2012): 23-27. https://doi.org/10.1016/j.ndteint.2012.08.009

[26] Bao, S., X. Liu, and D. Zhang. "Variation of residual magnetic field of defective U75V steel subjected to tensile stress." *Strain* 51, no. 5 (2015): 370-378. https://doi.org/10.1111/str.12147

[27] Fu, Meili, Sheng Bao, and Huangjie Lou. "Characterization of stress concentration by tangential component Hp (x) of metal magnetic memory signals." *Journal of Wuhan University of Technology-Mater. Sci. Ed.* 33, no. 6 (2018): 1486-1490. https://doi.org/10.1007/s11595-018-1995-5

[28] Yan, Chun-yan, Wu-shen Li, Xin-jie Di, Zhen-kui Xue, Shi-wu Bai, and Fang-ming Liu. "Variation regularity of metal magnetic memory signals with inspecting time-interval and location." *Journal of Central South University of Technology* 14, no. 3 (2007): 319-323. https://doi.org/10.1007/s11771-007-0063-7

[29] Chen, Changrong, Shoujin Zeng, and Liangyou Su. "Strain energy based method for metal magnetic memory effect of tensile tested structures." *Journal of Nondestructive Evaluation* 38 (2019): 1-12. https://doi.org/10.1007/s10921-019-0579-4

[30] Liu, Bin, Peng Fu, Ruifeng Li, Peng He, and Shiyun Dong. "Influence of crack size on stress evaluation of ferromagnetic low alloy steel with metal magnetic memory technology." *Materials* 12, no. 24 (2019): 4028. https://doi.org/10.3390/ma12244028

[31] Bai, Fang, and Bo Song. "Deformation Effects on Metal Magnetic Memory in API 5L X70 Steel." *Advanced Materials Research* 415 (2012): 2101-2104. https://doi.org/10.4028/www.scientific.net/AMR.415-417.2101

[32] Lihong, Dong, Xu Binshi, Dong Shiyun, Chen Qunzhi, and Wang Dan. "Variation of stress-induced magnetic signals during tensile testing of ferromagnetic steels." *Ndt & E International* 41, no. 3 (2008): 184-189. https://doi.org/10.1016/j.ndteint.2007.10.003

[33] Jian, Xingliang, Xingchao Jian, and Guoyong Deng. "Experiment on relationship between the magnetic gradient of low-carbon steel and its stress." *Journal of Magnetism and Magnetic Materials* 321, no. 21 (2009): 3600-3606. https://doi.org/10.1016/j.jmmm.2009.06.077

[34] Kumar, Arbind, and Ashok Misra. "Shape anisotropy of magnetic field generation during tensile fracture in steel." *Journal of Magnetism and Magnetic Materials* 285, no. 1-2 (2005): 71-78. https://doi.org/10.1016/j.jmmm.2004.07.017

[35] Huang, Haihong, Gang Han, Zhengchun Qian, and Zhifeng Liu. "Characterizing the magnetic memory signals on the surface of plasma transferred arc cladding coating under fatigue loads." *Journal of Magnetism and Magnetic Materials* 443 (2017): 281-286. https://doi.org/10.1016/j.jmmm.2017.07.067

[36] Hu, Zhibin, Jianchun Fan, Shengnan Wu, Haoyuan Dai, and Shujie Liu. "Characteristics of metal magnetic memory testing of 35CrMo steel during fatigue loading." *Metals* 8, no. 2 (2018): 119. https://doi.org/10.3390/met8020119

[37] Liu, Bin, Zeyu Ma, Luyao He, Di Wang, Hai Zhang, and Jian Ren. "Quantitative study on the propagation characteristics of MMM signal for stress internal detection of long distance oil and gas pipeline." *NDT & E International* 100 (2018): 40-47. https://doi.org/10.1016/j.ndteint.2018.08.006